

Synthesis and evaluation of novel flavonoid metal complexes as immune boosters for dual modulation of IL-6 pathway in SARS-CoV-2 therapy; A combined *in-silico* and *in-vitro* approaches

swaroop Krishna Akey

JSS College of Pharmacy Ooty

Sunil Kumar Patnaik

JSS College of Pharmacy Ooty

P Vasanth

JSS College of Pharmacy Ooty

MR Jeyaprakash

JSS College of Pharmacy Ooty

MR Praharsh Kumar

JSS College of Pharmacy Ooty

N Jawahar

JSS College of Pharmacy Ooty

Jubie Selvaraj (✉ jubie@jssuni.edu.in)



JSS College of Pharmacy Ooty <https://orcid.org/0000-0002-4633-6621>

Research Article

Keywords: IL-6, cytokine release syndrome, metal complexes, quercetin

Posted Date: May 3rd, 2022

DOI: <https://doi.org/10.21203/rs.3.rs-1525280/v1>

License:   This work is licensed under a Creative Commons Attribution 4.0 International License. [Read Full License](#)

Abstract

It is observed that cytokine release syndrome (CRS) is one of the major causes for the death of several COVID-19 patients. Though several cytokines are involved in CRS, Interleukin-6 (IL-6) modulation plays a major role. We aim to develop new flavonoid metal complexes as immune boosters targeting IL-6 for SARS-CoV-2 treatment. To find potential flavonoids, PyRx 0.9 tool has been used to dock 152 secondary plant metabolites against IL-6 (PDB ID: 1ALU). The top scorer flavonoid (quercetin) was made into quercetin-oxime. Seven metal complexes (QM-1 to QM-7) were made from quercetin-oxime by utilizing divalent metals such as zinc, copper, magnesium, cobalt, barium, and cadmium. Based on ADME profile, it was assumed that all compounds were moderately soluble and would not penetrate the BBB. The *in-vitro* hemolytic research revealed a modest hemolytic effect in all seven complexes. To control the IL-6 inhibitory potential, complexes were screened for cytotoxicity in cell lines MCF-7 which predominantly expresses the IL-6 level. The cytotoxic effects of all complexes were considerable relative to the marketable Nutridac formulation. The complex quercetin-Zinc (QM1) and quercetin-Zinc-Ascorbic acid (QM7) significantly affected MCF-7 cells in concentrations 43.25 and 48.54 µg/ml, respectively.

1. Introduction

The new data shows that the Coronavirus has been a fresh epidemic across the world for the last one and half years. In December 2019, it was initially identified in Wuhan, China. The Coronavirus is a massive family strain of the family of coronaviridae (Abbasifard and Khorramdelazad 2020). Firstly, this virus was transferred to people through infected animals (bats and pangolins) and then spread worldwide (del Rio and Malani 2020). Recent studies indicate that many individuals infected with COVID-19 may die due to their excessive response of immune systems, which leads to the abnormal production of cytokines known as cytokine release syndrome (CRS) (Wu et al. 2020; Tang et al. 2020). CRS affects the decline and deterioration of COVID-19 pneumonic patients who develop acute respiratory stress syndrome (ARDS) (Qin et al. 2020; Rana 2020). CRS is a systemic inflammatory response characterized by a significant increase of pro-inflammatory cell cytokines in response to infection, certain medicines, or specific other reasons (Shimizu 2019; Ji et al. 2020; Zhang et al. 2020). It is a term that denotes an overactive immune response that is characterized by the production of interferons, interleukins, tumour necrosis factor-alpha (TNF α), chemokines, and other proteins (Zhou et al. 2020; Wu et al. 2020; Qin et al. 2020; Sinha et al. 2020). CRS is a frequent immunopathogenesis that may result in acute respiratory distress syndrome (ARDS), sepsis, graft-versus-host disease (GvHD), rheumatoid arthritis-induced, macrophage activation syndrome (MAS), and primary and secondary hemophagocytic lymphohistiocytosis (HLH) (Liu et al. 2020). Numerous cytokines, including IL-6, IL-1, IL-2, IL-10, TNF α , and IFN γ , are implicated in the 'cytokine storm' in many COVID-19 patients; however, IL-6 seems to play a significant role, with increased levels associated with dyspnea, ARDS, and poor clinical outcomes (Han et al. 2020; Drewett et al. 2021). While the IL-6 cytokine plays a substantial function as an inflammatory mediator in both innate and adaptive immune responses, it may also have anti-inflammatory and protective properties in some clinical circumstances (Kang et al. 2019). New research on covid-19 patients indicates that IL-6 and its receptors may have significant diagnostic and therapeutic potential.

A potent pro-inflammatory agent, IL-6 works through two major signaling pathways: cis and trans. Cis-signaling involves IL-6 joining the membrane-bound IL-6 receptor and Gp130 to activate Janus kinases (JAKs) and signal transducer and activator of transcription 3 (STAT3) (Abbasifard and Khorramdelazad 2020). These pleiotropic effects on the acquired immune system (B and T cells) and the innate immune system (neutrophils, macrophages, and natural killer cells) may lead to CRS when activated. To activate trans-signaling, significant levels of IL-6 in the blood bind to the solubilized version of the receptor (sIL-6R) on most somatic cell types (Metcalf et al. 2020). To stimulate IL-6–sIL-6R–JAK-STAT3 signaling in cells lacking mIL-6R, such as endothelial cells, increases the "cytokine storm" by secreting VEGF, MCP-1, IL-8, and IL-6 while decreasing E-cadherin expression on endothelial cells. VEGF secretion and reduced E-cadherin expression led to vascular permeability and leakage, contributing to hypotension and pulmonary dysfunction in ARDS (Bousoik and Montazeri Aliabadi 2018; Masjedi et al. 2018; Rupasinghe 2020).

IL-6 and IL-6R antagonists have previously shown effectiveness in treating CRS and secondary hemophagocytic lymphohistiocytosis (sHLH), both of which cause blood cytokine elevation. This CRS implicates IL-6 in the pathogenesis of cytokine-driven hyperinflammatory disorders and makes it a possible COVID-19 target (Rana 2020). The increasing scientific evidence for flavonoids potential to relieve inflammatory diseases, as well as their safe and cost-effective characteristics, has led to the development of new flavonoid-inspired nutraceuticals and therapies. The deficit of metals impacts plasma cytokines such as TNF α and IL-1, IL-6 whereas metal supplementation has a dose-dependent effect (Foster and Samman 2012; Rupasinghe 2020). The goal is to design and produce novel flavonoid metal complexes as immune boosters for treatment with SARS-CoV-2. We report the synthesis, characterization, and cytotoxicity investigations of flavonoid metal complexes to build new "leads" which act as Interleukin-6 antagonists.

2. Materials And Methods

Solvents and reagents of analytical and laboratory-grade were used in the synthesis process. Chemicals were dried and cleaned by established procedures. TLC analysis was used to monitor the reactions and determine the purity of the products. We utilized 60-F 254 (0.5mm) MERCK aluminium back pre-coated silica gel plates for thin-layer analytical chromatography. Carousel Radleys Parallel organic synthesizer was used for the final synthesis. The absorbance of substances was determined using a Shimadzu UV-visible spectrometer. The FT-IR spectrometer from Perkin-Elmer was used to determine the IR spectra. The ^1H - and ^{13}C -NMR spectra were obtained using a BRUKER (400MHz FT-NMR) in DMSO solvent with TMS serving as an internal standard. Shimadzu LC-MS was used to determine the mass spectra of the compounds. Carbanio.com supplied quercetin (2-(3,4 dihydroxyphenyl)-3,5,7-trihydroxy-4H-chromen-4-one). All chemical products used in reagent preparation were weighed with an accuracy of 0,0001 g. Solvents were cleaned and dried in line with industry requirements.

2.1.1. Molecular docking

PyRx 0.8 was used to perform the docking research. PyRx is a Python-based programming language that runs on almost any contemporary machine, from personal computers to supercomputers. PyRx has been used to determine the binding affinity of a ligand to a protein in order to facilitate molecular docking. The workflow of our study is depicted in Fig. 1. PyRx, a structure-based docking program, was used to screen all 152 secondary metabolites for IL-6 (PDB: 1ALU) at a resolution of 1.90. Additionally, ligands for energy reduction interact in good ways. The MMFF94 force field performed the minimization in 200 steps with an RMS gradient of 0.1. Following the devaluation, the ligands were transferred to PDBQT format. First, we had chosen the macromolecule that will define the produced protein's binding site. Next, the active docking site was constructed utilizing bound ligand binding locations. Then, virtual screening was performed on a molecular window, with all produced ligands interacting with the specified active site (Trott and Olson 2009; Chen 2015). All ligands were categorized according to their binding affinity as determined by the PyRx score. Following that, the ligands were classified according to their binding energy levels. The top scorer quercetin was converted into imines, oximes, and hydrazides. The docking analysis for these analogues was then re-evaluated and re-constructed by the binding energy estimations.

2.1.2. ADME and Toxicity prediction

Using the SwissADME tool, ADME properties were estimated, and toxicity properties were calculated using the online bioinformatics tool PreADMET. ADMET studies were conducted for designed metal complexes, such as their aqueous solubility, blood-brain barrier (BBB), plasma protein binding (PPB), hepatotoxicity, and polar surface area, cytochrome P450, CYP2D6 inhibition, human gut absorbance, rodent carcinogenicity, Ames mutagenicity and toxicology potential development. A logP value that indicates lipophilicity in a molecule is the partition coefficient value in an octanol/water system. LogP is an important metric that reflects the impact on bioavailability, distribution, volume clearance, the permeability of the membrane. Diverse tissues have been investigated in this study with the expectations and significant characteristics of the compounds as mutagenicity and toxicity. The PreADMET serve has predicted pharmacologically relevant properties.

2.1.3. Synthesis of Quercetin oxime (QO)

A combination of hydroxylamine hydrochloride (0.01 mol, 0.69 g), quercetin (0.01 mol, 5.8 g), and sodium acetate trihydrate (0.01 mol, 1.36 g) diluted in 25 mL ethanol (0.01 mol) was heated at reflux on a water bath with continuous mixing for four hours. A yellow solid precipitated out during ambient temperature was filtered, cleaned, and dried it under a vacuum (Özyürek et al. 2014).

2.1.4. General Procedure for the synthesis of Quercetin oxime metal complexes (QM1-QM6)

The proposed metal complexes were synthesized using the metal salts $ZnCl_2$, $CuCl_2$, $CoCl_2$, $MgCl_2$, $BaCl_2$, and $CdCl_2$ in a 1:2 stoichiometric ratio. The quercetin oxime binder was dissolved in a metal salt solution in 10ml of ethanol and 10ml distilled water. Following this time, for the complete precipitation of the

produced compounds was kept at low temperatures (cooler) for two days before being filtered into a porous drying platform and sucked in a desiccator (da Silva et al. 2020).

2.1.5. General Procedure for the synthesis of Quercetin ascorbic acid metal complex (QM7)

One analogue was developed as a bi-ligand containing quercetin, zinc, and ascorbic acid in a 1:1:1 ratio. The complex was produced in a stoichiometric ratio of 1:1:1 using metal salt ZnCl₂ with quercetin and ascorbic acid as ligands. The quercetin and ascorbic acid binder were mixed with 10 mL ethanol, and the metal salt was dissolved in 10 mL distilled water, and the mixture was stirred continuously for 3 hours at room temperature. Following this, the solution was cooled at lower temperature (cooler) for two days before being filtered through a porous plate funnel and vacuum-sealed in a desiccator.

(4 Z)-2-(3,4-dihydroxyphenyl)-4-(hydroxyimino)-4 H -chromene-3,5,7-triol (QO)

Yellow crystal; R_f value = 0.78 (Toluene: Ethyl acetate: Formic acid. 5:4:0.2., v/v developer, visualization: UV and I₂), yield 91%. M.p 295–300°C. M.F: C₁₅H₁₁NO₇; MW: 317. UV-Visible (nm): 203, 256, 305, 374 (bands formed), FTIR (KBr, cm⁻¹): 3264.63 (O-H str), 1614.47 (C = N str), 1141.90 (C-OH str), 1169.87 (C-O-C str), 789.98 (C-H str Ar), 1558.54 (C = C str). ¹H NMR (300 MHz, DMSO) δ 10.04 (s, 1H, OH₁), 11.02 (s, 1H, OH₂), 9.4 (s, 1H, OH₅), 8.6 (s, 1H, OH₆), 7.9 (m, 5H, Ar-H₁), 7.7 (m, 5H, Ar-H₂), 12.72 (s, 1H, OH₃), 10.57 (s, 1H, OH₄) MS: 317.05(M⁺).

5,5'-bis(3,4-dihydroxyphenyl)-8,8',10,10'-tetrahydroxy-3,3'-spirobi[chromeno[4,3-e]1,3-dioxo-4-aza-2-zincacyclohexane]-3,3'-diuide (QM1)

Greenish black; R_f value = 0.52 (Toluene: Ethyl acetate: Formic acid. 5:4:0.2., v/v developer, visualization: UV and I₂), yield 85%. M.p > 300°C. M.F: ZnC₃₀H₁₈N₂O₁₄; MW: 694.006. UV-Visible (nm): 257, 298, 302, 375 (bands formed), FTIR (KBr, cm⁻¹): 3382.29 (O-H str), 1645.33 (C = N str), 1274.03 (C-OH str), 1086.92 (C-O-C str), 2975.30 (C-H str Ali), 1543.10 (C = C str), 879.57 (C-H str Ar), 668.38, 1047.38, 1391.69 (Zn-O). ¹H NMR (300 MHz, DMSO) δ 10.04 (s, 1H, OH₁), 9.8 (s, 1H, OH₂), 9.4 (s, 1H, OH₅), 8.6 (s, 1H, OH₆), 7.9 (m, 5H, Ar-H₁), 7.7 (m, 5H, Ar-H₂), 7.5 (s, 1H, OH₃), 7.14 (s, 1H, OH₄), 7.06 (s, 1H, OH₇), 6.9 (s, 1H, OH₈). MS: 694.006(M⁺).

5,5'-bis(3,4-dihydroxyphenyl)-3,3'-spirobi[chromeno[4,3-e]1,3-dioxo-4-aza-2-cupracyclohexane]-8,8',10,10'-tetrol (QM2)

Black powder; R_f value = 0.36 (Toluene: Ethyl acetate: Formic acid. 5:4:0.2., v/v developer, visualization: UV and I₂), yield 79%. M.p > 300°C. M.F: CuC₃₀H₁₈N₂O₁₄; MW: 693.001. UV-Visible (nm): 257, 297 (bands formed), FTIR (KBr, cm⁻¹): 3456.55 (O-H str), 1619.29 (C = N str), 1295.24 (C-OH str), 1114.89 (C-O-C str), 771.54 (C-H str Ar), 1558.54 (C = C str), 668.36, 1345.39 (Cu-O), ¹H NMR (300 MHz, DMSO) δ 10.07 (s, 1H, OH₁), 9.8 (s, 1H, OH₂), 9.5 (s, 1H, OH₅), 8.65 (s, 1H, OH₆), 7.8 (m, 5H, Ar-H₁), 7.7 (m, 5H, Ar-H₂), 7.5 (s, 1H, OH₃), 7.14 (s, 1H, OH₄), 7.06 (s, 1H, OH₇), 6.8 (s, 1H, OH₈) MS: 694.01(M⁺).

5,5'-bis(3,4-dihydroxyphenyl)-3,3'-spirobi[chromeno[4,3-e]1,3-dioxo-4-aza-2-magnasacyclohexane]-8,8',10,10'-tetrol (QM 3)

Yellow powder; Rf value = 0.21 (Toluene: Ethyl acetate: Formic acid. 5:4:0.2., v/v developer, visualization: UV and I₂), yield 86%. M.p > 300°C. M.F: MgC₃₀H₁₈N₂O₁₄; MW: 654.060. UV-Visible (nm): 203, 256, 302, 374 (bands formed), FTIR (KBr, cm⁻¹): 3461.38 (O-H str), 1654.01 (C = N str), 1263.42 (C-OH str), 1169.87 (C-O-C str), 721.40 (C-H str Ar), 1559.90 (C = C str), 459.07, 611.45, 1092.71 (Mg-O), ¹H NMR (300 MHz, DMSO) δ 10.06 (s, 1H, OH₁), 9.9 (s, 1H, OH₂), 9.5 (s, 1H, OH₅), 8.65 (s, 1H, OH₆), 7.8 (m, 5H, Ar-H₁), 7.68 (m, 5H, Ar-H₂), 7.5 (s, 1H, OH₃), 7.20 (s, 1H, OH₄), 7.06 (s, 1H, OH₇), 6.8 (s, 1H, OH₈) MS: 654.060(M⁺).

5,5'-bis(3,4-dihydroxyphenyl)-3,3'-spirobi[chromeno[4,3-e]1,3-dioxo-4-aza-2-cobaltacyclohexane]-8,8',10,10'-tetrol (QM4)

Yellow powder; Rf value = 0.42 (Toluene: Ethyl acetate: Formic acid. 5:4:0.2., v/v developer, visualization: UV and I₂), yield 86%. M.p > 300°C. M.F: BaC₃₀H₁₈N₂O₁₄; MW: 767.981. UV-Visible (nm): 256, 302, 374 (bands formed), FTIR (KBr, cm⁻¹): 3439.19 (O-H str), 1623.15 (C = N str), 1265.35 (C-OH str), 1169.87 (C-O-C str), 725.26 (C-H str Ar), 1557.57 (C = C str), 570.95, 639.42, 1028.09 (Co-O), ¹H NMR (300 MHz, DMSO) δ 10.05 (s, 1H, OH₁), 9.76 (s, 1H, OH₂), 9.39 (s, 1H, OH₅), 8.65 (s, 1H, OH₆), 7.8 (m, 5H, Ar-H₁), 7.6 (m, 5H, Ar-H₂), 7.5 (s, 1H, OH₃), 7.14 (s, 1H, OH₄), 7.06 (s, 1H, OH₇), 6.9 (s, 1H, OH₈) MS: 689.403(M⁺).

5,5'-bis(3,4-dihydroxyphenyl)-3,3'-spirobi[chromeno[4,3-e]1,3-dioxo-4-aza-2-baracyclohexane]-8,8',10,10'-tetrol (QM5)

Brown powder; Rf value = 0.64 (Toluene: Ethyl acetate: Formic acid. 5:4:0.2., v/v developer, visualization: UV and I₂), yield 86%. M.p > 300°C. M.F: CoC₃₀H₁₈N₂O₁₄; MW: 689.008. UV-Visible (nm): 256, 304, 373 (bands formed), FTIR (KBr, cm⁻¹): 3473.91 (O-H str), 1703.20 (C = N str), 1320.32 (C-OH str), 1169.87 (C-O-C stretching), 717.54 (C-H str Ar), 1618.33 (C = C stretch), 459.07, 644.25, 1002.05 (Ba-O), ¹H NMR (300 MHz, DMSO) δ 10.04 (s, 1H, OH₁), 9.8 (s, 1H, OH₂), 9.4 (s, 1H, OH₅), 8.6 (s, 1H, OH₆), 7.9 (m, 5H, Ar-H₁), 7.7 (m, 5H, Ar-H₂), 7.5 (s, 1H, OH₃), 7.14 (s, 1H, OH₄), 7.06 (s, 1H, OH₇), 6.9 (s, 1H, OH₈) MS: 767.797 (M⁺).

5,5'-bis(3,4-dihydroxyphenyl)-3,3'-spirobi[chromeno[4,3-e]1,3-dioxo-4-aza-2-cadmacyclohexane]-8,8',10,10'-tetrol (QM6)

Yellow powder; Rf value = 0.40 (Toluene: Ethyl acetate: Formic acid. 5:4:0.2., v/v developer, visualization: UV and I₂), yield 86%. M.p > 300°C. M.F: CdC₃₀H₁₈N₂O₁₄; MW: 743.979. UV-Visible (nm): 202, 257, 373 (bands formed), FTIR (KBr, cm⁻¹): 3277.17 (O-H str), 1653.05 (C = N str), 1237.78 (C-OH str), 1173.72 (C-O-C str), 745.51 (C-H str Ar), 1623.15 (C = C str), 506.33, 556.48, 1003.02 (Ba-O), ¹H NMR (300 MHz, DMSO) δ 10.07 (s, 1H, OH₁), 9.88 (s, 1H, OH₂), 9.3 (s, 1H, OH₅), 8.6 (s, 1H, OH₆), 7.9 (m, 5H, Ar-H₁), 7.7 (m, 5H, Ar-H₂), 7.5 (s, 1H, OH₃), 7.18 (s, 1H, OH₄), 7.1 (s, 1H, OH₇), 6.9 (s, 1H, OH₈) MS: 742.881 (M⁺).

6'-(1,2-dihydroxyethyl)-4-(3,4-dihydroxyphenyl)-7,9-dihydroxy-4'-oxo-4',6'-dihydro-9bH-spiro[1,3-dioxo-2-zincacyclopenta[4,5-c]chromene-2,2'-furo[3,4-d]1,3-dioxo-2-zincacyclopentane]-2,2-diide (QM7)

Yellow powder; Rf value = 0.27 (Toluene: Ethyl acetate: Formic acid. 5:4:0.2., v/v developer, visualization: UV and I₂), yield 84%. M.p > 300°C. M.F: ZnC₂₁H₁₆O₁₃; MW: 552.983. UV-Visible (nm): 224, 227, 236, 279 (bands formed), FTIR (KBr, cm⁻¹): 3442.09 (O-H str), 1704.17 (C = O str), 1249.91 (C-OH str), 1168.90 (C-O-C str), 2847.99 (C-H str Ali), 647.09 (C-H str Ar), 1575.89 (C = C str), 479.33, 515.01, 1020.38 (Zn-O), ¹H NMR (300 MHz, DMSO) δ 10.04 (s, 1H, OH₁), 9.8 (s, 1H, OH₂), 9.4 (s, 1H, OH₅), 8.6 (s, 1H, OH₆), 7.9 (m, 5H, Ar-H₁), 7.7 (m, 5H, Ar-H₂), 4.86 (s, 1H, OH₃), 3.45 (s, 1H, OH₄), 5.80 (d, 1H, Ar-H₃), 3.43 (s, 1H, Al-H₁), 3.45 (s, 1H, Al-H₂), 3.73 (s, 1H, Al-H₃) MS: 541.754 (M⁺).

2.2. Biological studies

2.2.1 Haemolytic Assay

A fresh blood sample from a retro-orbital rat was collected, spun for 10 minutes at 2000 rpm, and used to determine the haemolytic activity of produced compounds. The 0.9 percent NaCl solution was resuspended in the cell pellet to produce a 2 percent (v/v) cell suspension. A 100 µl suspension of red blood cells was added to the whole 96-well plate and incubated for 1 hour at 37°C with 5% CO₂. The release of haemoglobin was determined by spectrometric supernatant analysis at 540 nm as an indicator of red blood cell breakdown (RBC) (haemolysis). Complete haemolysis was obtained (positive control) by adding 1% (v/v) NaOH, while cells were negative in 0.9 percent (w/v) NaCl solution (Doshi and Une 2016).

2.2.2. Cell lines and culture medium

MCF-7 cell cultures were obtained from India's National Centre for Cell Sciences in Pune. The cells were cultured in Dulbecco's modified Eagle's medium (DMEM) supplemented with Fetal Calf Serum, trypsin (0.5g/L), EDTA (197.16mg/L), and PBS (1L) and maintained at 37°C in a CO₂ incubator. This solution was used to subculture adherent cells. After removing the medium, ten milliliters of trypsin/EDTA were added to this combination and incubated. In the flask, 10 ml DMEM medium was added and transferred to the centrifuge tube. For 5–7 minutes, the cells were spun at 1300–1500 rpm (Saleem et al. 2013).

2.2.3. MTT Assay

DMEM media with 10% FBS was used to trypsinize the monolayer cell culture and adjust the cell count to 1x10⁴ cells/well. 100µl of the diluted cell suspension (about 10,000 cells/well) was put to each well of a 96-well microtiter plate. The supernatant was discarded after 24 hours when a partial monolayer had developed. The monolayer was washed with medium once. Different concentrations of test samples (100µl) were applied to the partial monolayer in each well of microtiter plates. After that, the plates were incubated at 37°C for 72 hours in a 5% CO₂ environment. Every 24 hours, microscopic inspection and observations were made. After 72 hours, the sample solutions in the wells were removed, and each well was filled with 20µl of MTT (2 mg/ml) in MEM-PR (MEM without phenol red). The plates were gently shaken and incubated at 37°C in a 5% CO₂ environment for 3 hours. The supernatant was removed, and

50µl of isopropanol was added, followed by gentle shaking of the plates to dissolve the formazan produced. The absorbance was determined at a wavelength of 540 nm using a microplate reader. The percentage inhibition of cell growth was computed using the following formula, and the concentration of the medication or test sample required to inhibit cell growth by 50% was determined using the dose-response curves for each cell line (Saleem et al. 2013; Selvaraj et al. 2020).

$$\% \text{ Growth Viability} = \frac{\text{Mean OD of the individual test group}}{\text{Mean OD of the individual control group}}$$

3. Results And Discussion

3.1. In-silico design

The 3D structure of the protein human interleukin-6 was collected from the protein data bank (PDB: 1ALU). The active site amino acid residues were identified from the protein ligand interaction profile (PLIP). The amino acid residues present in a catalytic pocket are *Gln183, Phe78, Gln75, Ser76, Ala180, Arg179, Cys78, Glu69, Ser176, Met67, Gln175, Phe173, Lys171, Lys66, Pro65, Ser169, and Glu172* shown in **Figure 2**. The prepared protein was validated by the Ramachandran plot as shown in **Figure3**.

In PyRx, binding affinity parameters were considered for selecting the best "HITS" and compared with the known inhibitor Curcumin. PyRx binding energy is the energy of the interaction between the protein and the ligand. This value strongly indicates the extent of interaction of proteins and ligands. Quercetin (-6.9 kcal/mol) showed the highest binding affinity among all the 152 selected plant secondary metabolites whose binding energy was above standard curcumin (-5.8 kcal/mol) and co-crystal (tartaric acid) (-4.7 kcal/mol). Among the analogs designed, quercetin oxime (-7.0 kcal/mol) showed the highest binding affinity. The binding energy of top ten compounds and analogous was shown in **Table 1 and Table 2**. 2D interactions of quercetin IL-6 complex, quercetin oxime IL-6 complex, tartaric acid IL-6 complex were shown in **Figure 4 (a, b, c)**. Synthesised metal complexes were shown in **Table 3**. ADME properties of designed compounds (SwissADME) shown in **Table 4**. Toxicity studies for designed compounds (<http://preadmet.bmdrc.org/>) shown in **Table 5**.

3.2. Chemistry

We synthesized quercetin oxime from quercetin through the Beckmann rearrangement process, which converts the ketone to the ketoxime. The reaction is unusual in that no byproduct is produced. Metal complexes of quercetin oxime were produced from quercetin oxime in a 1:2 ratio using metal chlorides [ZnCl₂, CuCl₂, COCl₂, MgCl₂, BaCl₂, CdCl₂]. Quercetin oxime was able to form complexes with a variety of cations due to the presence of chelating sites in its structure. Chelating characteristics of quercetin oxime are dictated by their chemical structure, which consists of two aromatic rings benzoyl ring A and cinnamoyl ring B connected by an O-heterocycle. The 3-hydroxychromone, 4-N-hydroxychromone, and 3',4'-dihydroxyl groups are all potential chelating sites for scheme 1. They were made from quercetin and ascorbic acid using metal chlorides [ZnCl₂] in a 1:1:1 ratio. Quercetin and ascorbic acid may form

complexes with a variety of cations due to chelating sites in their structure. The molecular structure of quercetin determines its chelating properties: two aromatic rings (benzoyl ring A and cinnamoyl ring B) linked by an O-heterocycle. The 3',4'-dihydroxyl, and 5-hydroxychromone groups are potential chelating sites. The chelating effects of ascorbic acid are governed by its ring structure, with different hydroxy groups linked by O-heterocycle for scheme 2.

3.2. Biological studies

3.2.1. Haemolytic assay

The metal complexes were tested at various concentrations (25, 50, and 100 µg/ml) for haemolytic activity. 50 µg/ml showed little haemolysis. The explicit or implicit impact of chemicals on blood cells necessitates nanotoxicology research. The movement of erythrocytes through many organs damages DNA, membranes and causes birth defects. In this case, ligand biocompatibility testing was more important than chemical toxicity testing. **Table 6** shows the standard values for haemolytic test. **Table 7** shows that all substances were somewhat haemolytic, ranging from 2-10% of the haemolytic index. So, all produced compounds were safer.

3.2.2 Cytotoxicity studies

The metal complexes were tested for cytotoxicity using MCF 7 cells, which had high amounts of IL-6. QM1 and QM7 had significant cytotoxic effects on MCF-7 cells at 43.25 and 48.54 g/ml, respectively **Figure 5**. Our complexes were compared to the conventional medication Nutridac (Curcumin with metal salts), which showed 94.78g/ml. The quercetin oxime metal complexes exhibited dose-dependent viability of MCF-7 cells. **Table 8** shows that quercetin oxime compounds inhibit IL-6 in breast cancer cells without harming normal cells.

Conclusion

Flavonoid metal complexes produced in this study have the potential to serve as "lead molecules" in the suppression of IL-6 in cytokine storm in COVID-19 patients via an inhibitory action on the IL-6 receptor, in addition to performing immunomodulation. Further molecular research, maybe carried out in order to investigate the inhibitory capacity of IL-6. So, it may be inferred that the synthetic metal complexes QM1, QM7 are superior to Nutridac in terms of performance. In addition to IL-6 directed COVID-19, it is possible that these complexes will be utilized as "HITS" for the development of new molecules for the treatment of inflammatory auto-immune diseases such as rheumatoid arthritis, juvenile idiopathic arthritis, and giant cell arthritis in the future.

Abbreviations

IL-6 - Interleukin-6

CRS - cytokine release syndrome

SARS-CoV-2 - severe acute respiratory syndrome – Coronavirus

ARDS - Acute respiratory stress syndrome

TNF α - Tumour necrosis factor-alpha

GvHD - Graft-versus-host disease

MAS - Macrophage activation syndrome

HLH - Hemophagocytic lymphohistiocytosis

Gp130 – Glycoprotein-130

JAKs - Janus kinases

STAT3 - signal transducer and activator of transcription 3

VEGF – Vascular endothelial growth factor

TLC -Thin layer chromatography

BBB – Blood brain barrier

PPB - plasma protein binding

ADMET- Absorption, distribution, metabolism, elimination, toxicity

DMEM - Dulbecco's modified Eagle's medium

MTT - 3-(4,5-Dimethylthiazol-2-Yl)-2,5-Diphenyltetrazolium Bromide

PLIP - Protein ligand interaction profile

PDB - Protein data bank

Declarations

Conflict of Interest

The authors declare that no conflicts of interest.

Ethical Approval

This article does not contain any human participant and animal work.

Funding support

The present research work is funded by the “G. Rangachari memorial (PG pharmacy Fellowship) award” from the Tamilnadu pharmaceutical sciences welfare trust. Grant no: TNPSWT: 2021/2999.

Authors' contributions

All authors contributed equally.

Acknowledgment

Author Akey Krishna Swaroop expresses his gratitude to JSS College of Pharmacy, JSS Academy of Higher Education and Research.

References

1. Abbasifard M, Khorramdelazad H (2020) The bio-mission of interleukin-6 in the pathogenesis of COVID-19: A brief look at potential therapeutic tactics. *Life Sci* 257:118097. <https://doi.org/10.1016/j.lfs.2020.118097>
2. Bousoik E, Montazeri Aliabadi H (2018) “Do We Know Jack” About JAK? A Closer Look at JAK/STAT Signaling Pathway. *Front Oncol* 8:287. <https://doi.org/10.3389/fonc.2018.00287>
3. Chen Y-C (2015) Beware of docking! *Trends Pharmacol Sci* 36:78–95. <https://doi.org/10.1016/j.tips.2014.12.001>
4. da Silva WMB, de Oliveira Pinheiro S, Alves DR et al (2020) Synthesis of Quercetin-Metal Complexes, In Vitro and In Silico Anticholinesterase and Antioxidant Evaluation, and In Vivo Toxicological and Anxiolytic Activities. *Neurotox Res* 37:893–903. <https://doi.org/10.1007/s12640-019-00142-7>
5. del Rio C, Malani PN (2020) COVID-19—New Insights on a Rapidly Changing Epidemic. *JAMA* 323:1339. <https://doi.org/10.1001/jama.2020.3072>
6. Doshi GM, Une HD (2016) Quantification of Quercetin and Rutin from Benincasa hispida Seeds and Carissa Congesta Roots by High-performance Thin Layer Chromatography and High-performance Liquid Chromatography. *Pharmacognosy Res* 8:37–42. <https://doi.org/10.4103/0974-8490.171098>
7. Drewett GP, Copaescu A, Mouhtouris E et al (2021) Evolution of the Human Cytokine Response from Acute Illness to Disease Resolution in SARS-Cov-2 Infection—Implications for Therapeutic Monitoring and Therapeutic Targets. *J Clin Immunol* 41:1162–1164. <https://doi.org/10.1007/s10875-021-01039-x>
8. Foster M, Samman S (2012) Zinc and Regulation of Inflammatory Cytokines: Implications for Cardiometabolic Disease. *Nutrients* 4:676–694. <https://doi.org/10.3390/nu4070676>
9. Han H, Ma Q, Li C et al (2020) Profiling serum cytokines in COVID-19 patients reveals IL-6 and IL-10 are disease severity predictors. *Emerg Microbes Infections* 9:1123–1130. <https://doi.org/10.1080/22221751.2020.1770129>
10. Ji Y, Ma Z, Peppelenbosch MP, Pan Q (2020) Potential association between COVID-19 mortality and health-care resource availability. *The Lancet Global Health* 8:e480. [Page 11/19](https://doi.org/10.1016/S2214-</div><div data-bbox=)

11. Kang S, Tanaka T, Narazaki M, Kishimoto T (2019) Targeting Interleukin-6 Signaling in Clinic. *Immunity* 50:1007–1023. <https://doi.org/10.1016/j.immuni.2019.03.026>
12. Liu B, Li M, Zhou Z et al (2020) Can we use interleukin-6 (IL-6) blockade for coronavirus disease 2019 (COVID-19)-induced cytokine release syndrome (CRS)? *J Autoimmun* 111:102452. <https://doi.org/10.1016/j.jaut.2020.102452>
13. Masjedi A, Hashemi V, Hojjat-Farsangi M et al (2018) The significant role of interleukin-6 and its signaling pathway in the immunopathogenesis and treatment of breast cancer. *Biomed Pharmacother* 108:1415–1424. <https://doi.org/10.1016/j.biopha.2018.09.177>
14. Metcalfe RD, Putoczki TL, Griffin MDW (2020) Structural Understanding of Interleukin 6 Family Cytokine Signaling and Targeted Therapies: Focus on Interleukin 11. *Front Immunol* 11:1424. <https://doi.org/10.3389/fimmu.2020.01424>
15. Özyürek M, Akpınar D, Bener M et al (2014) Novel oxime based flavanone, naringin-oxime: Synthesis, characterization and screening for antioxidant activity. *Chemico-Biol Interact* 212:40–46. <https://doi.org/10.1016/j.cbi.2014.01.017>
16. Qin C, Zhou L, Hu Z et al (2020) Dysregulation of Immune Response in Patients With Coronavirus 2019 (COVID-19) in Wuhan, China. *Clin Infect Dis* 71:762–768. <https://doi.org/10.1093/cid/ciaa248>
17. Rana MM (2020) Cytokine storm in COVID-19: Potential therapeutics for immunomodulation. *J Res Clin Med* 8:38–38. <https://doi.org/10.34172/jrcm.2020.038>
18. Rupasinghe HPV (2020) Special Issue “Flavonoids and Their Disease Prevention and Treatment Potential”: Recent Advances and Future Perspectives. *Molecules* 25:4746. <https://doi.org/10.3390/molecules25204746>
19. Saleem K, Wani WA, Haque A et al (2013) Synthesis, DNA binding, hemolysis assays and anticancer studies of copper(II), nickel(II) and iron(III) complexes of a pyrazoline-based ligand. *Future Med Chem* 5:135–146. <https://doi.org/10.4155/fmc.12.201>
20. Selvaraj J, John JBA, Joghee NM et al (2020) Coumarin-Fatty Acid Conjugates as Potential ER α /AKT-1 Antagonists for ER Positive Breast Cancer. *ACAMC* 20:437–449. <https://doi.org/10.2174/1871520619666191028104339>
21. Shimizu M (2019) Clinical Features of Cytokine Storm Syndrome. In: Cron RQ, Behrens EM (eds) *Cytokine Storm Syndrome*. Springer International Publishing, Cham, pp 31–41
22. Sinha P, Matthay MA, Calfee CS (2020) Is a “Cytokine Storm” Relevant to COVID-19? *JAMA Intern Med* 180:1152. <https://doi.org/10.1001/jamainternmed.2020.3313>
23. Tang Y, Liu J, Zhang D et al (2020) Cytokine Storm in COVID-19: The Current Evidence and Treatment Strategies. *Front Immunol* 11:1708. <https://doi.org/10.3389/fimmu.2020.01708>
24. Trott O, Olson AJ (2009) AutoDock Vina: Improving the speed and accuracy of docking with a new scoring function, efficient optimization, and multithreading. *J Comput Chem* NA-NA. <https://doi.org/10.1002/jcc.21334>

25. Wu C, Chen X, Cai Y et al (2020) Risk Factors Associated With Acute Respiratory Distress Syndrome and Death in Patients With Coronavirus Disease 2019 Pneumonia in Wuhan, China. *JAMA Intern Med* 180:934. <https://doi.org/10.1001/jamainternmed.2020.0994>
26. Zhang C, Wu Z, Li J-W et al (2020) Cytokine release syndrome in severe COVID-19: interleukin-6 receptor antagonist tocilizumab may be the key to reduce mortality. *Int J Antimicrob Agents* 55:105954. <https://doi.org/10.1016/j.ijantimicag.2020.105954>
27. Zhou F, Yu T, Du R et al (2020) Clinical course and risk factors for mortality of adult inpatients with COVID-19 in Wuhan, China: a retrospective cohort study. *The Lancet* 395:1054–1062. [https://doi.org/10.1016/S0140-6736\(20\)30566-3](https://doi.org/10.1016/S0140-6736(20)30566-3)

Tables

Table 1-3 are available in the Supplemental Files section.

Table 4. ADME properties of designed compounds.

Sample code	Solubility ^a	BBB ^b	CYP2D6 ^c	Synthetic accessibility ^d	Absorption ^e	WlogP ^f	TPSA ^g
QM1M1	Moderately soluble	No	No	5.92	Low	3.11	241.94
QM2	Moderately soluble	No	No	5.97	Low	3.11	241.94
QM3	Moderately soluble	No	No	5.4	Low	3.11	241.94
QM4	Moderately soluble	No	No	5.83	Low	3.11	241.94
QM5	Moderately soluble	No	No	5.51	Low	3.11	241.94
QM6	Moderately soluble	No	No	5.91	Low	3.11	241.94
QM7	Soluble	No	No	5.82	Low	0.38	193.83

a) Solubility b) BBB- Blood-Brain Barrier c) CYP2D6- Cytochrome 450 inhibition d) Synthetic accessibility e) Absorption f) WlogP- Partition coefficient of octanal/water system g) TPSA- Total Polar surface area.

Table 5. Toxicity studies for designed compounds.

Sample code	Algae test	hERG inhibition	TA100_10RLI	TA1535_10RLI	TA1535_NA	Daphnia
QM1M1	0.000144202	Medium risk	negative	negative	negative	0.00569073
QM2	0.000237045	Medium risk	negative	negative	negative	0.0111477
QM4	0.000257791	Medium risk	negative	negative	negative	0.01631
QM6	0.000237295	Medium risk	negative	negative	negative	0.0107329
QM7	0.0282117	Medium risk	negative	negative	negative	0.798832
Limit	<1	--	--	--	--	<1

Table 6. Standard values of Haemolytic assay

Haemolytic index (%)	Haemolytic grade
0-2	Non-haemolytic
2-10	Slightly haemolytic
10-20	Moderately haemolytic
20-40	Markedly haemolytic
>40	haemolytic

Table 7. Haemolytic assay of synthesized compounds.

Compound	Concentration	Absorbance	Haemolytic %
Q	100	2.974	5.217%
	50	2.775	4.713%
	25	1.437	1.326%
QM4	100	2.933	5.113%
	50	2.843	4.886%
	25	1.961	2.653%
QM7	100	3.323	6.101%
	50	3.063	5.443%
	25	2.673	4.455%
QM2	100	3.209	5.812%
	50	2.898	5.025%
	25	2.369	3.754%
DMSO		0.851	0%

Table 8. Cytotoxicity study of the metal complexes.

S.no	Sample code	concentration	% Growth inhibition	CTC ₅₀ (µg/ml)
1	QM1	500	74.09	43.25
		250	68.32	
		125	60.89	
		62.5	56.12	
		31.25	44.89	
2	QM7	500	73.80	48.54
		250	69.35	
		125	62.98	
		62.5	53.98	
		31.25	42.98	
3	Std-1 (Nutridac)	500	65.98	94.78
		250	60.12	
		125	54.89	
		62.5	43.56	
		31.25	34.32	

Scheme

Scheme 1 and 2 are available in supplementary section.

Figures

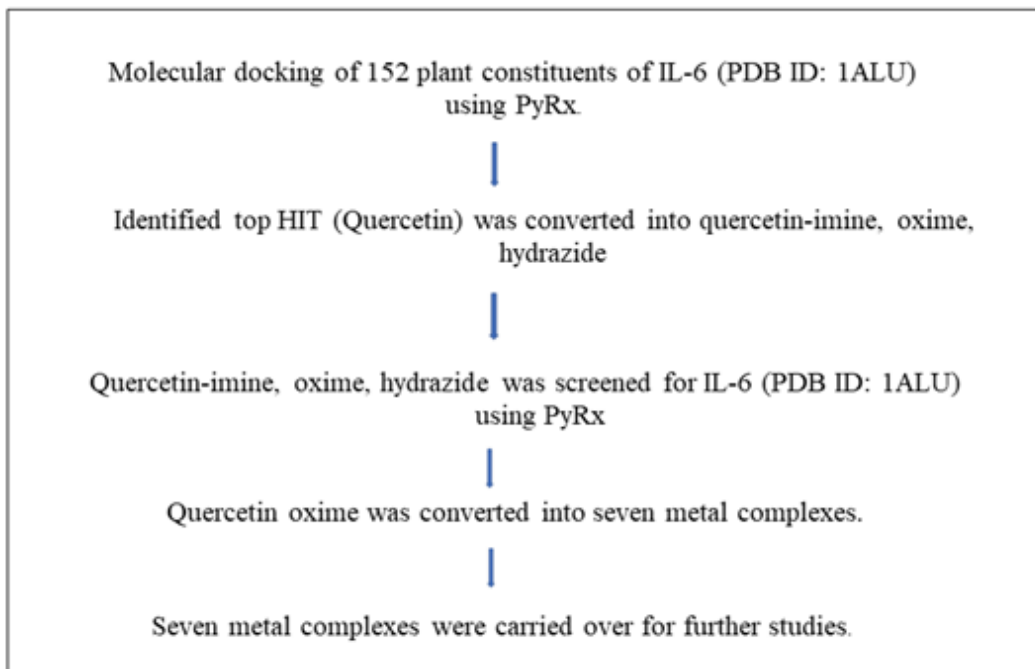


Figure 1

Work flow of our study.

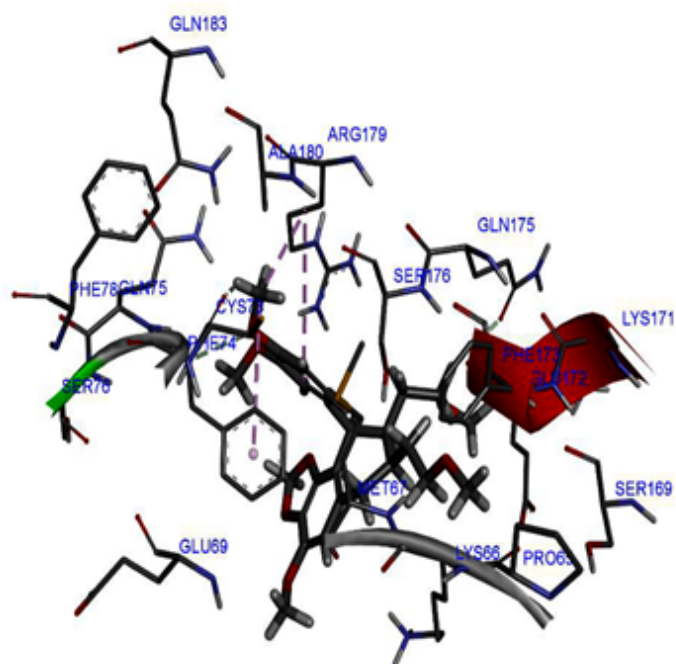


Figure 2

Amino acids present in the active site of the catalytic pocket of the IL-6 receptor (PDB id: 1ALU)

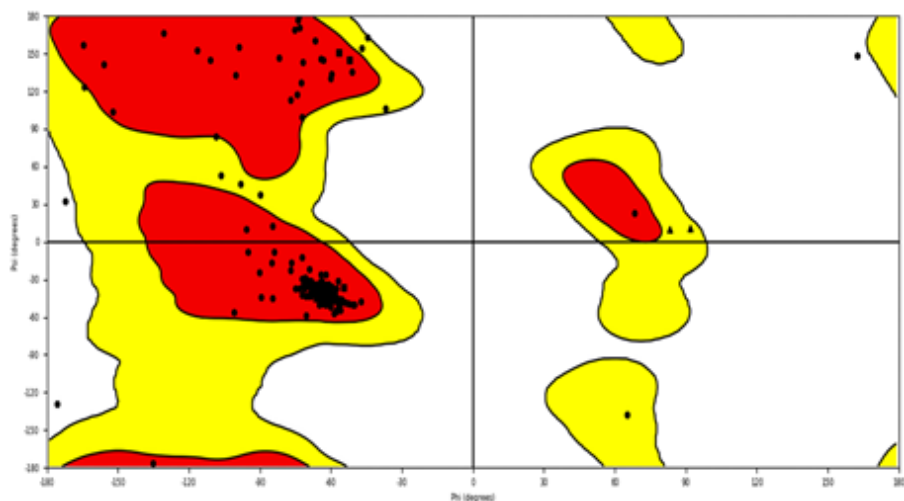


Figure 3

Ramachandran plot of 1ALU

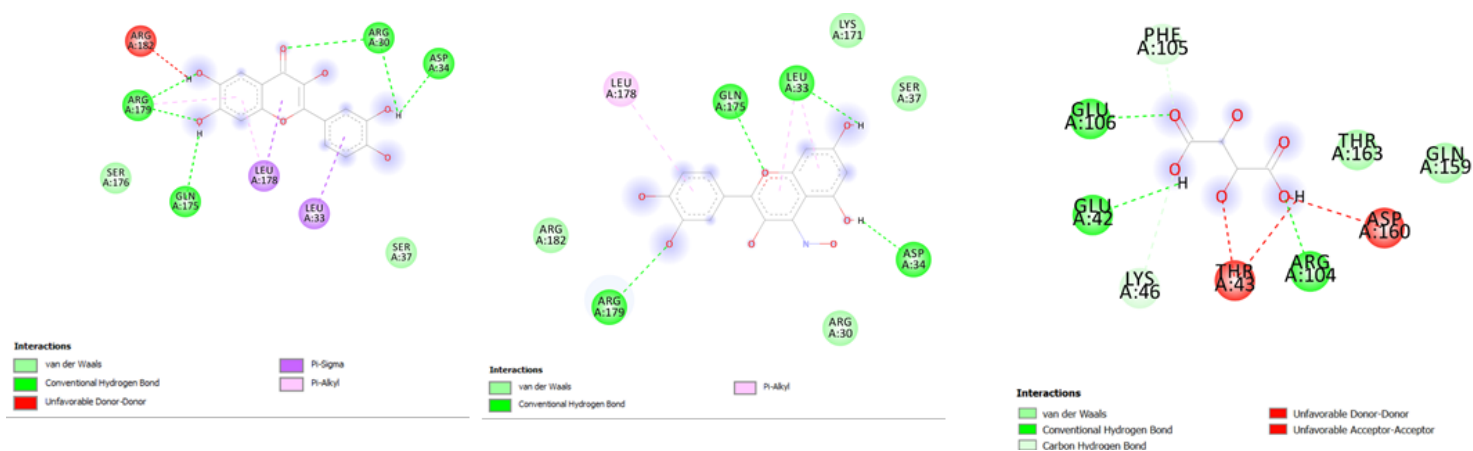
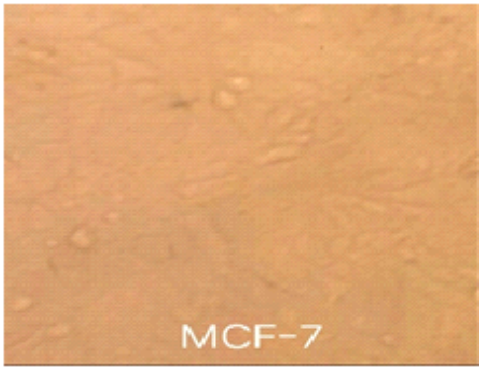


Figure 4

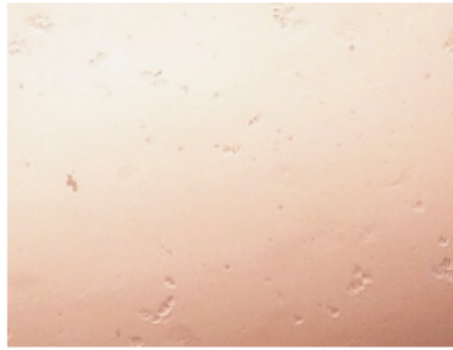
(a). 2D interaction of Quercetin IL-6 complex.

(b). 2D interaction of Quercetin oxime IL-6 complex.

(c). 2D interaction of Tartaric acid IL-6 complex.



a



b

Figure 5

a) MCF-7 cell line without adding drug.

b) MCF-7 cell line inhibition after addition of drug.

Supplementary Files

This is a list of supplementary files associated with this preprint. Click to download.

- [Scheme01.png](#)
- [Scheme02.png](#)
- [Tables13.docx](#)